Available online at www.sciencedirect.com

ScienceDirect

Ceramics International 40 (2014) 155–162

CERAMICS INTERNATIONAL

www.elsevier.com/locate/ceramint

High frequency electrical transport properties of $CoFe_2O_4$ and $Sr_2NiMnFe_{12}O_{22}$ composite ferrites

Attia Aslam[a], M.U. Islam[a,*], Irshad Ali[a], M.S. Awan[b], Muhammad Irfan[a], Aisha Iftikhar[a]

[a]*Department of Physics, Bahauddin Zakariya University, Multan 60800, Pakistan*
[b]*Center for Micro and Nano Devices, Department of Physics, COMSATS Institute of Information Technology, Islamabad, Pakistan*

Received 6 March 2013; received in revised form 24 May 2013; accepted 30 May 2013
Available online 5 June 2013

Abstract

Composite ferrite ceramic materials were obtained by mixing sol/gel derived $CoFe_2O_4$ and $Sr_2NiMnFe_{12}O_{22}$ nanopowders sintered at 1050 °C for 3 h. The synthesized samples were characterized by XRD, Scanning Electron Microscopy, FT-IR, electrical resistivity and dielectric measurements. XRD analysis revealed that there is no new phase observed, indicating that no chemical reaction occurs between spinel and hexagonal phases and the intensity of Y-phase gradually decreased by increasing spinel concentration. Crystallite size calculated from XRD data decreased by increasing spinel concentration. Room temperature resistivity and activation energies of the samples increased with increasing spinel concentration. Dielectric constant of pure Y-type hexagonal ferrite decreased by increasing spinel concentration up to ~8.5. At higher frequency further decrease in dielectric constant was observed due to Maxwell-Wagner type relaxation with few resonance peaks beyond 2 GHz. Imaginary part of dielectric constant showed the similar behavior with frequency. Low dielectric constant, low dielectric losses and high resistivity make these composite ferrites useful in electromagnetic attenuation materials and microwave devices.

Keywords: Hexaferrite composites; Sol–gel; Resistivity; Permitivity; SEM

1. Introduction

The increasing exploitation of microwave (MW) frequencies for telecommunication has increased electromagnetic interference (EMI), pollution and stimulated the development of MW absorbers. Absorption of EM waves occurs in magnetic materials due to the magnetic losses. Ferrites exhibit substantial magnetic losses in the vicinity of their ferromagnetic resonance (FMR). Because of this they are one of the best materials for MW absorption [1]. Spinel ferrites are preferred for its high permeability while hexagonal ferrites have extremely high ferromagnetic resonance frequency in the GHz range. A little research work has been reported to prepare composite materials of spinel and hexagonal ferrite in order to utilize advantages of both materials [2]. Hence composite ferrites could be adjusted in a wide region of frequency from several megahertz up to several hundreds of megahertz [3]. Recently multilayer chip inductors (MLCI) used in the hyperfrequency regions have been rapidly developed as surface mounting devices (SMD). Incorporating spinel into hexagonal ferrites could improve the densification of the composite ferrites at relatively low temperatures [4,5]. Components made from composite ferrites can work stably in a wide temperature region from −20 up to 120 °C, and have dc resistivities larger than 10^{10} Ω-cm. This meets the requirement for fabrications of components by electroplate processing [2]. Due to larger resistivity and medium high frequency region, the composite ferrites are becoming promising medium for components used at medium high frequencies, such as micro-transformers and MLCI etc [6]. In the present paper different compositions of the composite ferrite system of xCo-Fe_2O_4+yMnNiY where the ratio of x:y is 1, 5 and 10 were prepared and investigated thoroughly.

*Corresponding author. Tel.: +92 61 9210343; fax: +92 61 9210068.
E-mail address: muislampk@yahoo.com (M.U. Islam).

0272-8842/$ - see front matter © 2013 Elsevier Ltd and Techna Group S.r.l. All rights reserved.
http://dx.doi.org/10.1016/j.ceramint.2013.05.116

2. Materials and methods

2.1. Preparation of composite ferrites

$CoFe_2O_4$ spinel ferrite was prepared by sol–gel auto-combustion technique. Stoichiometric amount of $Fe(NO_3)_3.9\ H_2O$ and $Co(NO_3)_2 \cdot 6H_2O$ and PEG (Polyethylene glycol with a molecular weight of 62.07 g/mole) was dissolved in deionized water and mixed in a 500 ml beaker. The pH value of the solution was adjusted to 7 to avoid the occurrence of harmful nitrogen dioxide during the process of heat treatment. The dark brown solution obtained was dried at 80 °C on hot plate to get a brown porous gel. The gel was then ignited and calcined at 950 °C for 8 h in order to get $CoFe_2O_4$ ferrite nanopowder with grain size of about 78.33 nm.

Y-type hexagonal ferrite with nominal composition of $Sr_2NiMnFe_{12}O_{22}$(MnNiY) was prepared by mixing the solutions obtained by dissolving the stoichiometric amount of $MnCl_2 \cdot 3H_2O$, $NiCl_2 \cdot 6H_2O$, $Sr(NO_3)_2$, $Fe(NO_3)_3 \cdot 9H_2O$ and $C_3H_4OH(COOH)_3$ in deionized water. Ignited gel was calcined at 1100 °C for 8 h to get ferrite powder with grain size 59.8 nm.

Both these kinds of ferrite powders were mixed together so as to get homogenous mixture. The proportions chosen were 1:1, 5:1, and 10:1 in terms of weight ratio of $CoFe_2O_4$:MnNiY. The composite ferrite samples with the proportions above were named C_1, C_2 and C_3, respectively. Appropriate amount of Bi_2O_3 was introduced as sintering aid. The mixed powders were sintered at 1050 °C for 3 h. All the samples were pressed into disks with the addition of 5 wt% PVA as a binder for characterization.

2.2. Characterization

The crystal structure was determined using JDX-3532 JEOL diffractometer which was operated at 40 kV and at 30 mA equipped with Cu-K_α ($\lambda = 1.5418$ Å) with Ni filter. JSM-5910 SEM was used for the study of morphology of all the samples. The FT-IR measurements were performed by using box furnace, thermo-scientific Nicolet Model 6700. DC electrical resistivity was measured by using two probe method. Keithley source meter model 2400 was used for resistivity measurements. The permittivity of the samples was measured using Agilent impedance analyzer model E4991 A RF.

3. Results and discussions

3.1. Phase identification

The XRD patterns of the ferrite samples are shown in Fig. 1. All the peaks were indexed by comparing JCPDS Cards no. 01-079-1743, 01-072-0749 for MnNiY ferrite and 00-001-1121, 00-001-1108 for $CoFe_2O_4$ ferrite.

It is apparent that all the composites consist of two phases: hexagonal (peak labeled as Y) and spinel (peak labeled as S). The absence of any new phase proved that there is no chemical reaction between spinel and hexagonal ferrites [7]. It is

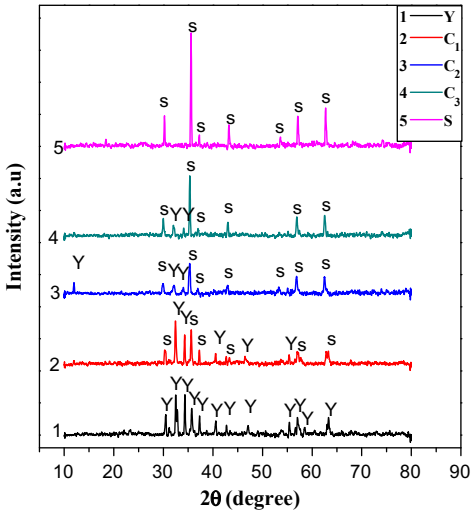

Fig. 1. X-ray Diffraction patterns of $CoFe_2O_4$(S) and $Sr_2NiMnFe_{12}O_{22}$ (MnNiY) ferrites and their composites: C_1, C_2, C_3.

observed that intensity of Y-phase gradually decreases by increasing spinel concentration in $Sr_2NiMnFe_{12}O_{22}$ however spinel peaks seems to be gradually dominating. Lattice parameters a, c and volume of the unit cell for $Sr_2NiMnFe_{12}O_{22}$ and $CoFe_2O_4$ tabulated in Table 1 are in good agreement with the reported results [8,9]. Crystallite size for each sample was calculated from XRD patterns by using the well-known Scherrer formula [10] and the values are listed in Table 1. The observed crystallite size for composites is smaller than the pure MnNiY and $CoFe_2O_4$ ferrites because the addition of $CoFe_2O_4$ in MnNiY inhibits the grain growth.

3.2. Microstructure

The SEM micrographs of the samples are shown in Fig. 2. Fig. 2 (a,b) shows the platelet grains of hexagonal ferrite and the spherical grains of spinel ferrite respectively. $CoFe_2O_4$ particles fill homogeneously in the interspaces arising due to irregular alignment of Y-type hexagonal platelet grains [11]. The grain size decreased by increasing the spinel concentration in the composite ferrites as listed in Table 1 is quite consistent with the reported results [12]. Due to interaction of $CoFe_2O_4$ and MnNiY inter-particle mass transport of $CoFe_2O_4$ or MnNiY is hindered and therefore, grain growth of both compositions becomes difficult [3]. Also the segregation of Bi_2O_3 at grain boundaries inhibits the grain growth and diffusion of MnNiY into grains besides lowering the sintering temperature [11].

3.3. FT-IR spectra

The FT-IR spectra of sintered samples in the wave number range 200–4000 cm^{-1} is shown in Fig. 3. In spinel ferrites, the absorption band around 600 cm^{-1} is attributed to stretching vibrations of tetrahedral complexes and the band around 400 cm^{-1} is attributed to octahedral complexes [13] The absorption bands of Co–O and Fe–O bonds appeared at

Table 1
Crystallite size, lattice parameters, cell volume, grain size, dielectric constant, resistivity, product of square root of resistivity and dielectric constant, and *n*-values of $Sr_2NiMnFe_{12}O_{22}$ (MnNiY), $CoFe_2O_4$ and C_1, C_2, C_3.

Composition	D (nm) Scherrer	a (Å)	c (Å)	c/ a	V(Å^3)	Grain Size (μm)	ε′ at 1 GHz	ρ (Ω-cm)	ε′ $\sqrt{\rho}$ at 1 GHz	*n*-Values
$Sr_2NiMnFe_{12}O_{22}$	59.80	5.908	43.155	7.304	1304.457	1.11	22.589	1.01×10^5	0.718×10^5	0.8975
$CoFe_2O_4$	78.33	8.372	–	–	586.982	3.65	11.971	1.00×10^8	2.88×10^5	0.6182
C_1	45.56	–	–	–	–	1.22	8.971	1.39×10^8	1.19×10^5	0.9711
C_2	45.55	–	–	–	–	0.99	7.324	1.85×10^8	1.05×10^5	0.9705
C_3	29.28	–	–	–	–	0.89	4.349	4.41×10^7	9.96×10^5	0.9971

399.2 and 528.8 cm^{-1} which are in quite expected range confirming the spinel $CoFe_2O_4$ structure, consistent with the XRD results [14]. Similarly bands at about 418 and 542.2 cm^{-1} in Sr_2NiMn $Fe_{12}O_{22}$(Y) are interpreted as the M-O stretching vibrations of hexaferrite and confirmed the formation of hexagonal structure, consistent with the XRD results [15,16]. The difference in band position is expected because of difference in Fe^{3+}–O^{2-} distance for octahedral and tetrahedral sites [17], however absorption bands for composite C_1, C_2, C_3 appeared at 406.4, 547.7, 410.5 and 542.6, 399.2 and 535.09 cm^{-1} respectively indicating absorption bands due to lattice vibration modes of M–O bonds as reported in [14–16].

3.4. DC resistivity measurement

3.4.1. Room temperature resistivity

The DC-electrical resistivity was measured by the two-point probe method using the relation mentioned in [18].

$$\rho = RA/h \tag{1}$$

where R is the resistance, h is thickness and $A = \pi r^2$ is the area of the pellet of the sample having radius r. Fig. 4 shows the room temperature resistivity vs. spinel concentration. The resistivity values have been tabulated in Table 1. It is observed that resistivity increases with the spinel addition from 1.01×10^5 to 1.85×10^8 Ω-cm. Generally resistivity increases with the decrease in grain size in polycrystalline materials. Smaller grains produce large number of insulating grain boundaries which act as barriers for hopping electrons. Due to smaller grains, grain-to-grain surface contact area also become smaller and therefore a lesser probability of electron hoping [12]. In the present case, the mean grain size of composite samples is comparatively lower than that of pure MnNiY ~1.11 μm and $CoFe_2O_4$ ~3.65 μm. Since cobalt ferrites have higher resistivity than MnNiY ferrites, therefore the addition of $CoFe_2O_4$ in MnNiY ferrite results in enhancement of resistivity of composite samples. Since Bi_2O_3 was added as sintering aid in composite ferrites and it is reported [19] that Bi^{5+} may act as scattering centers for the carriers hopping between two octahedral sites, that hinders the hopping mechanism between Fe^{2+} and Fe^{3+} ions and results in an increase of resistivity. For applications in microwave devices highly resistive materials are required [20]. The increase in resistivity results in material's diminution of eddy current losses that make them useful in radio frequency circuits, high quality filters, rod antennas and transformer cores [21].

3.4.2. Temperature dependent resistivity

Arrhenius plots for all the samples measured in the temperature range 303–453 K are shown in Fig. 5. It is clear from the figure that dc resistivity is decreasing linearly with temperature for all the samples according to the following relation [22].

$$\rho = \rho_o \exp\left(\mathrm{Ea}/\ k_B T\right) \tag{5.5}$$

where Ea is the activation energy of the charge carriers, ρ_o is the constant, T is the absolute temperature, k_B is the

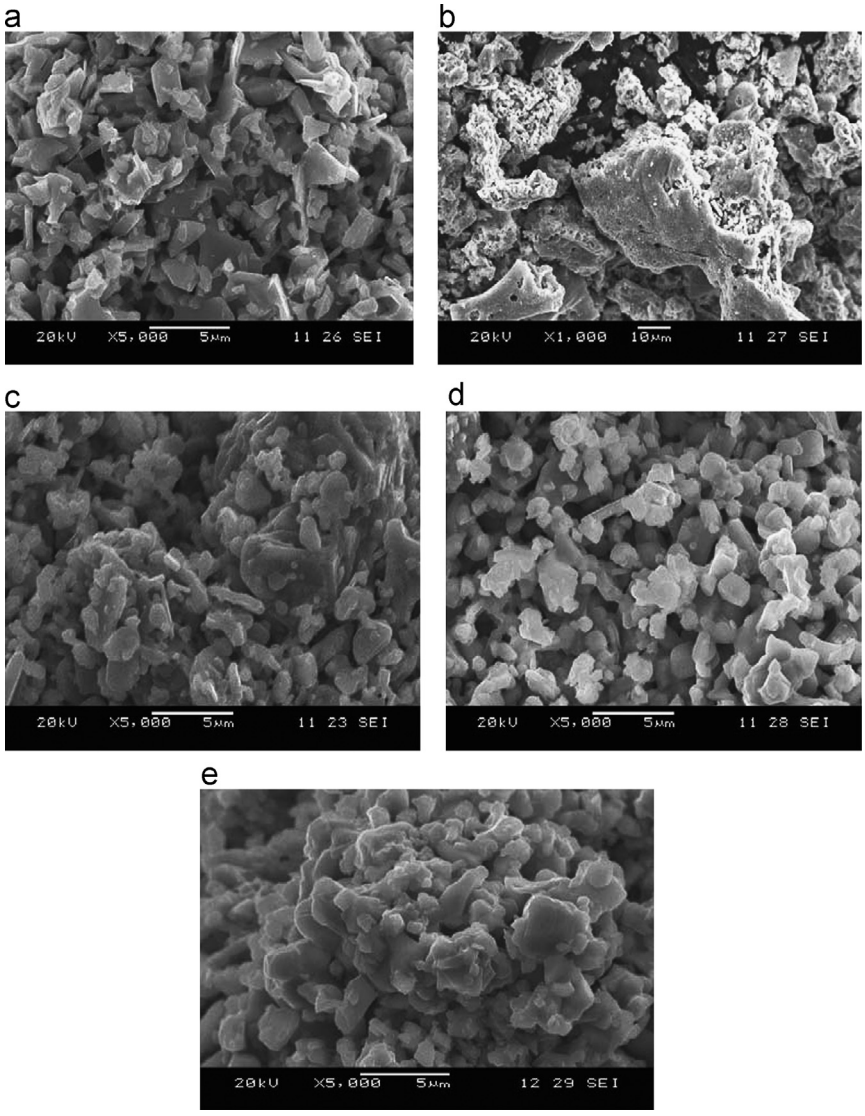

Fig. 2. SEM profiles of (a) $Sr_2NiMnFe_{12}O_{22}$ (MnNiY), (b) $CoFe_2O_4$ (S), (c) C_1 (d) C_2 and (e) C_3.

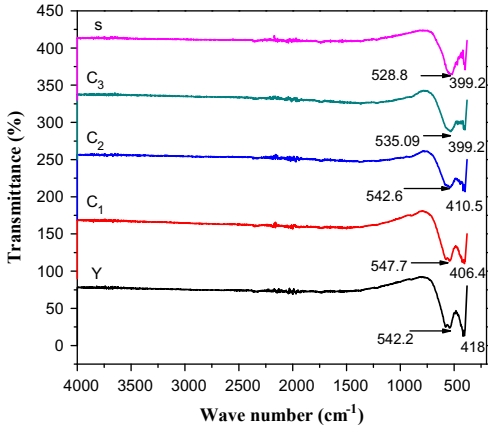

Fig. 3. FT-IR spectra for $CoFe_2O_4$ (S) and $Sr_2NiMnFe_{12}O_{22}$ (MnNiY) ferrites and their composites: C_1,C_2,C_3.

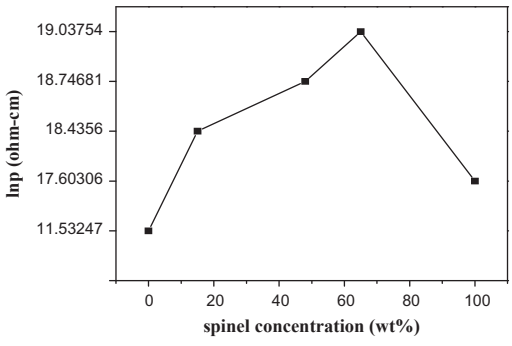

Fig. 4. Plot of room temperature resistivity vs. spinel concentration (wt%) for $CoFe_2O_4$ (S) $Sr_2NiMnFe_{12}O_{22}$ (MnNiY) ferrites and their composites: C_1, C_2, C_3.

Boltzmann's constant, indicating the semiconducting behavior of these samples. This can be attributed to thermally activated mobility of charge carriers. Impurities are responsible for conduction in ferrites at room temperature, while polaron hopping is the main conduction mechanism at higher temperatures. According to verwey, "the electronic conduction in ferrites is due to hopping of electrons between ions of same element present in more than one valence state, distributed

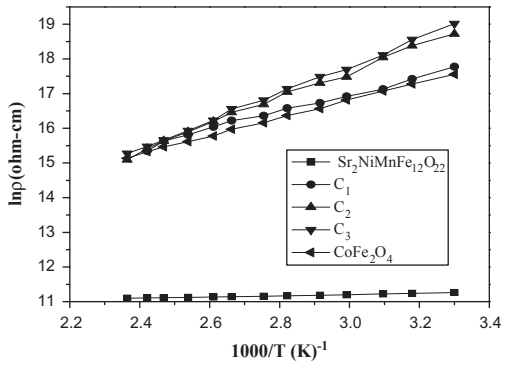

Fig. 5. Arrhenius plots for $CoFe_2O_4$ (S) $Sr_2NiMnFe_{12}O_{22}$ (MnNiY) ferrites and their composites: C_1, C_2, C_3.

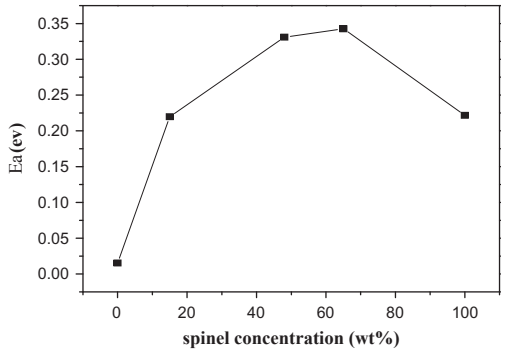

Fig. 6. Plot of activation energy vs. spinel concentration for $CoFe_2O_4$ (S) $Sr_2NiMnFe_{12}O_{22}$ (MnNiY) ferrites and their composites: C_1, C_2, C_3.

randomly over crystallographically different lattice sites" [23]. The values of activation energies ranges from 0.015 eV to 0.34 eV indicating that hopping is due to electrons as well as polarons [24]. The hopping probability depends upon the separation between the ions involved and the activation energy [23].

3.4.3. Activation energy

From the slope of Arrhenius plots the activation energies were calculated and are plotted in Fig. 6 as a function of spinel concentration. This variation is similar to the compositional variation of DC resistivity indicating that the sample with higher resistivity has higher values of activation energies and vice versa [25].

3.5. Dielectric properties

3.5.1. Dielectric constant

The relative speed that an electromagnetic signal can travel in a material is determined by the dielectric constant of that material. The speed of microwaves decreases when microwaves enter in a dielectric material, by a factor nearly equal to the square root of the dielectric constant [26]. Fig. 7 shows the variation of dielectric constant vs. frequency from MHz to 3 GHz range. There is a gradual decrease in dielectric constant with few resonance peaks observed at higher frequencies. Initial dispersion in dielectric constant is mainly due to the relaxation

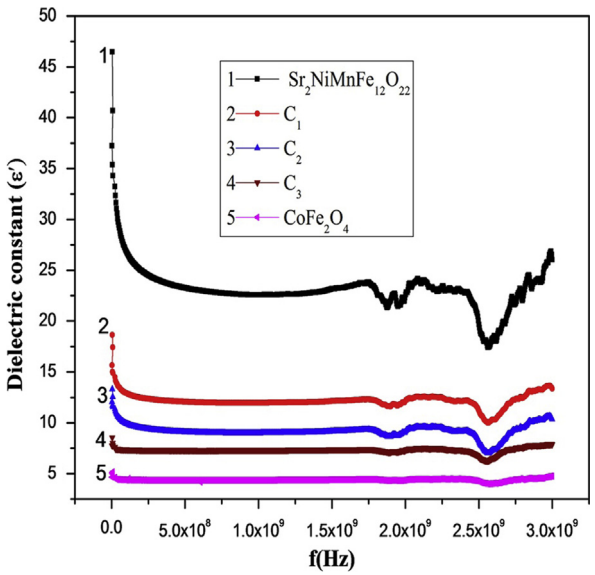

Fig. 7. Dielectric constant vs. frequency for $CoFe_2O_4$ (S) $Sr_2NiMnFe_{12}O_{22}$ (MnNiY) ferrites and their composites (C_1, C_2, C_3).

of dipoles; however the matching of the frequency of the applied field and the frequency of charge transfer between Fe^{2+} and Fe^{3+} can produce resonance at higher frequencies [27]. During sintering non-uniform distribution of oxygen ions at grains and grain boundaries results in interfacial polarization which is the one reason for dielectric properties in ferrites however at high frequencies dipolar, ionic, electronic polarization respectively contributes to dielectric constant [28,29]. Since the polarization reduces the field inside the medium. Hence dielectric constant decreases by increase in frequency [30]. Dipolar and ionic polarizations are the dominating mechanisms contributing to dielectric properties in ferrites in radio (MHz) to microwave (GHz) frequency range. In real materials, at microwave frequency and beyond, resonance peaks are observed due to undamped dipoles. However strongly damped dispersions are observed below microwave frequency [29]. Just like Maxwell–Wagner model in which there are two layers in the dielectric structure of ferrites. First conductive layer at higher frequencies consist of large number of grains is separated by other high resistive thin layer (grain boundaries) at low frequencies. Electronic exchange between Fe^{2+} and Fe^{3+} results is polarization in ferrites which is similar to conduction process. At higher frequencies this hoping of electron from Fe^{2+} and Fe^{3+} becomes difficult with the alternating frequency due to which the net displacement of charge in one direction decreases and therefore the dielectric constant decreases. However the high dielectric constants at low frequencies may be due to impurities, voids, moisture, dislocations and density. In Koops model for heterogeneous dielectrics the reason for the dispersion in the dielectric constant is that the electrons can respond to the changes in applied electric field only if the time required for hopping is less than half the period of the alternating field [26,28,31]. According to Iwauchi large number of Fe^{2+} ions at octahedral sites increase the electronic transfer between Fe^{2+} and Fe^{3+} and

Table 2
Relaxation time for main relaxation peaks in dielectric constant, dielectric loss and tangent loss.

Composition	Dielectric constant			Dielectric loss			Tangent loss		
	τ_1(ns)	τ_2(ns)	τ_3(ns)	τ_1(ns)	τ_2(ns)	τ_3(ns)	τ_1(ns)	τ_2(ns)	τ_3(ns)
$Sr_2NiMnFe_{12}O_{22}$	0.0849	0.0810	0.0615	0.0879	0.0822	1.07	0.0873	0.0821	1.06
C_1	0.0845	0.0829	0.0616	0.0878	1.19	–	0.0875	1.21	–
C_2	0.0845	0.0828	0.0615	0.0877	1.20	–	0.0876	1.19	–
C_3	0.0843	0.0819	0.0617	0.0882	1.16	–	0.0881	1.48	–
$CoFe_2O_4$	0.0846	0.0812	0.0616	0.0878	1.01	–	0.0874	1.20	–

results in higher values of dielectric constant [32]. Since spinel ferrites are soft ferrites and have smaller dielectric constant than hexagonal ferrites that may be one reason for decrease in dielectric constants in composite ferrites by addition of $CoFe_2O_4$ in $Sr_2NiMnFe_{12}O_{22}$. Moreover the mixing of $CoFe_2O_4$ in $Sr_2NiMnFe_{12}O_{22}$ suppress the grain growth and gives rise to smaller grain size, which results in enhancement of grain boundaries which is attributed to decrease in dielectric constant [33]. Due to increasing skin effect, the penetration depth of electromagnetic waves is decreased by high dielectric constant; however low dielectric constant at higher frequencies make ferrites applicable at higher frequencies [31]. Since by mixing $CoFe_2O_4$ in MnNiY dielectric constant and dielectric losses decrease it is useful for applications in microwave devices [21]. The condition for observing resonance in these curves is given, [28].

$$\omega\tau \sim 1 \quad (1)$$

where $\omega = 2\pi f_{max}$ and τ is the relaxation time that is related to the jumping probability per unit time, p, by an equation $\tau = 1/2p$ or [34]

$$f_{max} \alpha\, p \quad (2)$$

Relaxation time for each main relaxation peaks is shown in Table 2.

3.5.2. Relationship between dielectric constant and resistivity

The values of dielectric constant and resistivity are listed in Table 1. It can be observed from the table that the dielectric constant is approximately inversely proportional to the square root of resistivity in all the samples, while the product $\varepsilon'\sqrt{\rho}$ nearly remains constant as shown in Table 1. Almost same results were observed by Ishaque et.al [13].

3.5.3. Dielectric loss

Fig. 8 shows the behavior of dielectric loss as a function of increasing frequency which is quite similar to real part of the dielectric constant that can be explained according to smith and wijn that there is a inverse relation between the ratio of complex dielectric permittivity to ac conductivity with the applied field [35]. Materials having high conductivity generally have high dielectric losses and vice versa because in ferrites the dielectric losses are generally reflected in the conductivity measurements [36,37]. Relaxation time for each main relaxation and resonance peak is shown in Table 2.

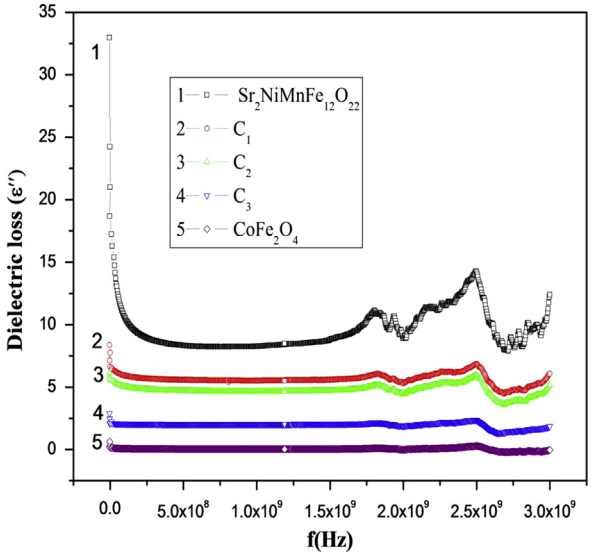

Fig. 8. Dielectric loss vs. frequency for $CoFe_2O_4$ (S) $Sr_2NiMnFe_{12}O_{22}$ (MnNiY) ferrites and their composites (C_1, C_2, C_3).

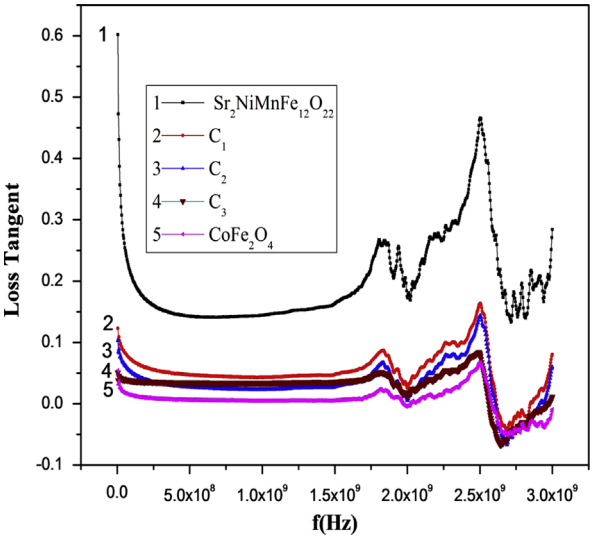

Fig. 9. Dielectric loss tangent vs. f(Hz) for $CoFe_2O_4$ (S) $Sr_2NiMnFe_{12}O_{22}$ (MnNiY) ferrites and their composites (C_1, C_2, C_3).

3.5.4. Dielectric loss tangent

Fig. 9 shows the variation of dielectric loss tangent (tan δ) with frequency. The decrease in tan δ is due to the fact that the hopping of electron between Fe^{3+} and Fe^{2+} do not follow the

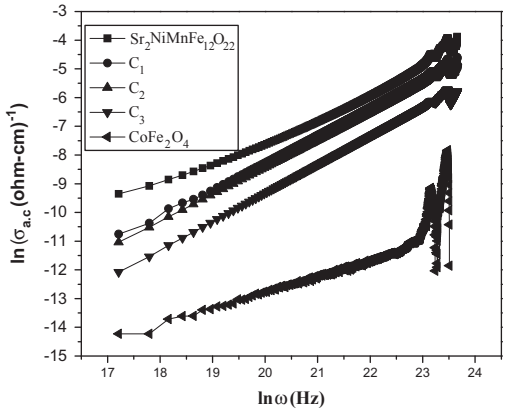

Fig. 10. ln $\sigma_{a.c}$ vs. lnω(Hz) for $CoFe_2O_4$ (S) $Sr_2NiMnFe_{12}O_{22}$ (MnNiY) ferrites and their composites: C_1, C_2, C_3.

frequency of the alternating electric field [38]. Peak in the graph appear because of the strong correlation between conduction and the dielectric behavior in the ferrite, because when the hopping frequency of the electrons between the ions with different chemical valence approximately approach to external electric field, peaks are observed in the graphs [39]. It is clear from figure that in composites, tan δ decreases by increasing spinel concentration, because the increase in resistivity results reduction in tan δ [40]. Several factors affect the value of tanδ such as stoichiometry, structural homogeneity, which in turn depend on composition and sintering temperature of the samples [41]. According to Maxwell–Wagner theory both έ and tanδ are inversely proportional with frequency [42]. Low dielectric losses are required for low core loss in ferrites and energy dissipation in the dielectric system is represented by Dielectric loss factor (tan δ) [31]. Relaxation time for the main dispersion peaks are shown in Table 2.

3.5.5. AC conductivity

Plot of logarithmic conductivity Vs logarithmic frequency is shown in Fig. 10. The AC conductivity (σ_{ac}) was determined using formula [35];

$$\sigma_{ac} = 2\pi f \varepsilon_o \varepsilon'' \tag{5.6}$$

It can be observed that conductivity increases with increasing frequency. Maxwell–Wagner model or heterogeneous model of the polycrystalline structure of ferrites (Koops 1951) can be used to explain this behavior. By increasing the frequency of applied field, the conductive layer become more active and hence promote the hopping of electron between Fe^{2+} and Fe^{3+} ions, thereby increases the hopping frequency and hence the conductivity. The dispersion in conductivity can be explained by Koop's theorem in which ferrite compacts were considered as multilayer capacitor, where ferrite grains and grain boundaries have different properties. With frequency the effect of the multilayer condenser rises which enhance the conductivity [43]. Resonance peaks at high frequency are due to the same reason as described in the previous section. Materials exhibiting high losses have high conductivity and vice versa because the dielectric losses in ferrite is generally reflected in the conductivity measurements [31]. The conduction mechanism in ac conductivity may be determined according to the equation [44];

$$\sigma(\omega) = B\omega^n \tag{5.7}$$

Slope of the line plotted between lnσ versus lnω equal to the exponent 'n' and intercept equal to lnB on vertical axis at ln $\omega = 0$. Electrical conduction will be dc conduction or frequency independent if $n = 0$ and if $n \leq 1$ electrical conduction will be frequency dependent or ac conduction. In our case the values of n lies between 0.6182 and 0.9971 as shown in Table 1, that indicates that the studied samples follows charge hopping mechanism and exhibit ac conduction [44].

4. Conclusions

SEM results revealed, increase of density with spinel concentration due to homogeneous distribution of $CoFe_2O_4$ and filling in the interspace produced due to irregular alignment of the hexagonal platelet grains of MnNiY matrix. The room temperature dc electrical resistivity of the composite ferrites was found to increase from 1.00×10^8 to 1.85×10^8 (Ω-cm), which is an important objective to make them useful in core materials. Temperature dependence of dc resistivity showed the semiconducting behavior of all the samples. Activation energy of the composite ferrites was greater as compared to pure ferrites, which indicated that samples with higher resistivity have higher activation energy and vice versa. Dielectric constant decreased with increase in spinel concentration which makes them good electromagnetic radiation absorbing materials due to reduction in skin effect. Due to electronic exchange between Fe^{2+} and Fe^{3+} permittivity decreased with increase of frequency consistent with Maxwell-Wagner model. Imaginary part of permittivity and loss tangent showed normal behavior of dielectrics with frequency for all the samples. Ac conductivity increased with frequency but decreased with spinel concentration. The conductivity mechanism determined is of hopping type.

References

[1] D. Lisjak, V.B. Bregar, A. Znidarsic, M. Drofenik, Microwave behaviour of ferrite composites, Journal of Optoelectronics and Advanced Materials 8 (1) (2006) 60–65.

[2] Weiguo Qu, XiaoHui Wang, Longtu Li, Preparation and performance of NiCuZn–Co_2Y composite ferrite material, Material Science and Engineering B99 (2003) 274–277.

[3] Weiguo Qu, XiaoHui Wang, Longtu Li, Preparation and performance of NiCuZn–CO_2Z composite Ferrite material, Journal of Magnetism and Magnetic Materials 257 (2003) 284–289.

[4] Hongguo Zhang, Longtu Li, Zhenwei Ma, Ji Zhou, Zhenxing Yue, Zhilun Gui, Investigation on permeability-frequency characteristics and microstructure of composite ferrites, Journal of Magnetism and Magnetic Materials 218 (2000) 67–71.

[5] Hongguo Zhang, Longtu Li, Pinggui Wu, Ji Zhou, Zhenwei Ma, Zhilun Gui, Investigation on structure and properties of low-temperature sintered composite ferrite, Materials Research Bulletin 35 (2000) 2207–2215.

[6] Yang Bai, Ji Zhou, Zhilun Gui, Longtu Li, Lijie Qiao, The physical properties of Bi–Zn co-doped Y-type hexagonal ferrite, Journal of Alloys and Compounds 450 (2008) 412–416.

[7] Weiguo Qu, Xiao Hui Wang, Longtu Li, Preparation and performance of NiCuZn–Co_2Y composite ferrite material, Material Science and Engineering B 99 (2003) 274–277.
[8] M.Y. Salunkhe, D.K. Kulkarni, Structural, magnetic and microstructural study of $Sr_2Ni_2Fe_{12}O_{22}$, Journal of Magnetism and Magnetic Materials 279 (2004) 64–68.
[9] Montana Sangmanee, Santi Maensiri, Nanostructures and magnetic properties of cobalt ferrite($CoFe_2O_4$) fabricated by electrospinning, Applied Physics A 97 (2009) 167–177.
[10] B.D. Cullity, Elements of X-ray diffraction, Notre Dame, Indiana (1977) 90–91.
[11] Hongguo Zhang, Longtu Li, Pinggui Wu, Ji Zhou, Zhenwei Ma, Zhilun Gui, Investigation on structure and properties of low-temperature sintered composite ferrite, Materials Research Bulletin 35 (2000) 2207–2215.
[12] A. Verma, T.C. Goel, R.G. Mendiratta, R.G. Gupta, High-resistivity nickel-zinc ferrites by the citrate precursor method, Journal of Magnetism and Magnetic Materials 192 (1999) 271–276.
[13] M. Ishaque, M.U. Islam, M. Azhar Khan, I.Z. Rahman, A. Genson, S. Hampshire, Structural, electrical and dielectric properties of yttrium substituted nickel ferrites, Physica B 405 (2010) 1532–1540.
[14] Mahmoud Goodarz Naseri, Elias B. Saion, Hossein Abbastabar A hang ar, Abdul Halim Shaari, Mansor Hashim, Simple synthesis and characterization of cobalt ferrite nanoparticles by a thermal treatment method, Journal of Nanomaterials 2010 (2010) 8, Article ID 907686, http://dx.doi.org/10.1155/2010/907686.
[15] Han Zhidong, Dong Limin, Wu Ze, Zhang Xianyou, Structure of $BaLa_xFe_{12-x}O_{19}/SiO_2$ synthesized by sol–gel method, Journal of Rare Earths 24 (2006) 75.
[16] Ihsan Ali, M.U. Islam, M.S. Awan, Mukhtar Ahmad, Effects of Cr–Ga substitution on structural and magnetic properties of hexaferrite ($BaFe_{12}O_{19}$) synthesized by sol–gel auto-combustion route, Journal of Alloys and Compounds 547 (2013) 118–125.
[17] Mukhtar Ahmad, Ihsan Ali, Faiza Aen, M.U. Islam, Muhammad Naeem Ashiq, Shabbar Atiq, Waheed Ahmad, M.U. Rana, Effect of sintering temperature on magnetic and electrical properties of nano-sized Co_2W hexaferrites, Ceramics International 38 (2012) 1267–1273.
[18] Muhammad Javed Iqbal, Saima Farooq, Could binary mixture of Nd–Ni ions control the electrical behavior of strontium–barium M-type hexaferrite nanoparticles?, Materials Research Bulletin 46 (2011) 662–667
[19] Hassan Mehmood Khan, Misbah-ul Islam, Irshad Ali, Mazhar-ur-din Rana, Electrical transport properties of Bi_2O_3-doped $CoFe_2O_4$ and $CoHo_{0.02}Fe_{1.98}O_4$ ferrites, Material Sciences and Application 2 (2011) 1083–1089.
[20] Muhammad Naeem Ashiqa, Muhammad Javed Iqbal, Muhammad Najam-ul-Haq Pablo Hernandez Gomez, Ashfaq Mahmood Qureshi, Synthesis, magnetic and dielectric properties of Er–Ni doped Sr-hexaferrite nanomaterials for applications in high density recording media and microwave devices, Journal of Magnetism and Magnetic Materials 324 (2012) 15–19.
[21] Muhammad Javed Iqbal, Rafaqat Ali Khan, Shigemi Mizukami, Terunobu Miyazaki, Tailoring of structural, electrical and magnetic properties of $BaCo_2W$-type hexaferrites by doping with Zr–Mn binary mixtures for useful applications, Journal of Magnetism and Magnetic Materials 323 (2011) 2137–2144.
[22] M.U Islam, Faiza Aen, B Shahida, M Niazi, Azhar khan, T.Abbas Ishque, M.U. Rana, Electrical transport properties of CoZn ferrite-SiO_2 composites prepared by co-precipitation technique, Materials Chemistry and Physics 109 (2008) 482–487.
[23] Asghari Maqsood Shahid Hussain, Structural and electrical properties of Pb-doped Sr-hexa ferrites, Journal of Alloys and Compounds 466 (2008) 293–298.
[24] A.A. Sattar, Temperature dependence of electrical resistivity and thermo electric power of re substituted Cu–Cd ferrite, Egyptian Journal of Solids 26 (2) (2003) 113–121.
[25] B. Ramesh, D. Ravinder, Electrical properties of Li–Mn ferrites, Materials Letters 62 (2008) 2043–2046.
[26] M. Anis-ur-Rehman, G. Asghar, Variation in structural and dielectric properties of co-precipitated nanoparticles strontium ferrites due to value of pH, Journal of Alloys and Compounds 509 (2011) 435–439.
[27] J. Chand, S. Verma, P . Kumar, M. Singh, Structural, electric and dielectric properties of $MgFe_2O_4$ ferrite processed by solid state reaction technique, International Journal of Theoretical and Applied Science 3 (2) (2011) 8–9.
[28] Sukhleen Bindra Narang, I.S Hudiara, Microwave dielectric properties of M-Type barium, calcium and strontium hexa-ferrite substituted with Co and Ti, Journal of Ceramic Processing Research 2 (7) (2006) 113–116.
[29] P.J. Harrop, Dielectrics, Butterworths, London, 1972.
[30] S.F. Mansour, Frequency and composition dependence on the dielectric properties for Mg–Zn ferrite, Egyptian Journal of Solids 2 (28) (2005) 263–272.
[31] Muhammad Javed Iqbal, Muhammad Naeem Ashiq, Iftikhar Hussain Gul, Physical, electrical and dielectric properties of Ca-substituted strontium hexaferrite ($SrFe_{12}O_{19}$) nanoparticles synthesized by co-precipitation method, Journal of Magnetism and Magnetic Materials 322 (2010) 1720–1726.
[32] Muhammad javed Iqbal, Muhammad Naeem Ashiq, Pablo Hernandez-Gomez, Jose Maria Munos, Synthesis, physical, magnetic and electrical properties of Al–Ga substituted Co-precipitated nanocrystallline strontium hexaferrite, Journal of Magnetism and Magnetic Materials 320 (2008) 881–886.
[33] Lijun Jia, Jun Luo, Huaiwu Zhang, Yulan Jing, Yu Shi, Effect of Y_2O_3 additive on the microstructure and high-frequency properties of Z-type hexaferrites, Journal of Magnetism and Magnetic Materials 321 (2009) 77–80.
[34] G. Ranga Mohan, D. Ravinder, A.V. Ramana Reddy, B.S. Boyanov, Dielectric properties of polycrystalline mixed nickel–zinc ferrites, Materials Letters 40 (1999) 39–45.
[35] G.F.M. Pires, H.O. Rodrigues Junior, J.S. Almeida, E.O. Sancho, J.C. Goes, M.M. Costa, J.C. Denardin, A.S.B. Sombra, Study of the dielectric and magnetic properties of Co_2Y, Y-type hexaferrite($Ba_2Co_2Fe_{12}O_{22}$) added with PbO and Bi_2O_3 in the RF frequency range, Journal of Alloys and Compounds 493 (2010) 326–334.
[36] Muhammad Naeem Ashiq, Muhammad Javed Iqbal, Iftikhar Hussain Gul, Structural, magnetic and dielectric properties of Zr–CD substituted strontium hexaferrite ($SrFe_{12}O_{22}$) nanoparticles, Journal of Alloys and Compounds 487 (2009) 341–345.
[37] I.H Gull, A. Maqsood, Structural, magnetic and electrical properties of cobalt ferrites prepared by the sol–gel route, Journal of Alloys and Compounds 465 (2008) 227–231.
[38] Muhammad Javed Iqbal, Muhammad Naeem Ashiq, Pablo Hernandez-Gomez, Jose Maria Munos, Synthesis, physical, magnetic and electrical properties of Al–Ga substituted Co-precipitated nanocrystallline strontium hexaferrite, Journal of Magnetism and Magnetic Materials 320 (2008) 881–886.
[39] Jian-Ping Zhou, Li Lv, Xian-Zhi Chen, Dielectric and magnetic properties of ZnO-doped cobalt ferrite, Journal of Ceramic Processing Research 2 (11) (2010) 263–272.
[40] A.M. Shaikh, S.S. Bellad, B.K. Chougule, Temperature and frequency-dependent dielectric properties of Zn substituted Li–Mg ferrites, Journal of Magnetism and Magnetic Materials 195 (1999) 384–390.
[41] Muhammad Naeem Ashiq, Muhammad Javed Iqbal, Iftikhar Hussain Gul, Effect of Al–Cr doping on the structural, magnetic and dielectric properties of strontium hexaferrite nanomaterials, Journal of Magnetism and Magnetic Materials 323 (2011) 259–263.
[42] Craig Ramesh Peelamedu, Dinesh Grimes, Agrawal, Rustum Roy, Ultralow dielectric constant nickel–zinc ferrites using microwave sintering, Journal of Materials Research 10 (18) (2003) 2292–2295.
[43] B. Lestrie, A. Maazouz, J.F. Gerard, H. Sautereau, G. Boiteux, G. Seytre, David E. Kranbuehl, Is the Maxwell–Sillars–Wagner model reliable for describing the dielectric properties of a core–shell particle-epoxy system?, Polymer 39 (26) (1998) 6733–6742
[44] E.E. Tanrıverdi, A.T. Uzumcu, H. Kavas, A. Demir, A. Baykal, Conductivity study of polyaniline-cobalt ferrite (PANI-$CoFe_2O_4$) nanocomposite, Nano-Micro Letters 3 (2) (2011) 99–107.